

Limitations of the Fourier Transform for Describing Test Course Profiles

Alexander Steinwolf, University of Auckland, Auckland, New Zealand

William H. Connon III, U.S. Army Aberdeen Test Center, Aberdeen, Maryland

Following previous efforts at the Aberdeen Test Center, further work has been undertaken on analysis and simulation of test course terrain that military vehicles are required to negotiate during developmental and operational testing. The surface roughness vertical displacement as a function of distance travelled is treated similarly to acceleration time histories. However, instead of the familiar power spectral density, a Wave Number Spectrum (WNS) is computed in the spatial domain. Until now, any inverse Fourier transform conversion of WNS into the terrain data has been carried out within the limits of the Gaussian random model whereas actual surface roughness is often a non-Gaussian process. It is shown in this article that when a synthetic spatial history with a given course WNS is generated by Gaussian procedures, the simulation obtained can lose severity compared to real terrain data. A number of test courses have been analysed and additional characteristics such as probability density function, kurtosis, skewness and crest factor have been considered. Various non-Gaussian features in many course profiles were discovered. To simulate terrain data with the correct skewness and kurtosis, the Hermite polynomial method of nonlinear transformation was used and the non-Gaussian probability density of synthetic terrain data has been achieved both in the central section and at the tails.

The Aberdeen Test Center (ATC) provides and maintains several test courses representing the Army's ground vehicle transportation environment. The courses are monitored to ensure 'constant' roughness and the existence of certain specific features for each. To do this, the terrain profiles of the ATC test courses are measured regularly using a profilometer based on a special purpose trailer. The profilometer makes a series of displacement and angular measurements that lead to computation of surface roughness as a function of distance traveled over the test course.

Measurements are made at constant increments (normally 3 in.) over the length of the test course. These uniformly sampled, digitized values are analogous to the digitization of acceleration signals in the time domain. Thus, many of the standard analysis techniques that are common in the time domain become applicable in the spatial domain. For example, if a characteristic similar to the Power Spectral Density (PSD) in the time domain would be introduced in the spatial domain and calculated for the course profile measured, then synthetic terrain data could be digitally generated by a procedure analogous to the inverse Fourier transform in the time domain.

The course profile data obtained are of use in computer dynamic models¹ and multi-actuator servo-hydraulic rigs for testing entire vehicles.² If initial recordings themselves are taken, their length is restricted and not comparable with the necessary duration of durability tests. Hence, in such a situation, there is no other technique except repetition of the same test profile. From this point of view, the inverse Fourier transform procedure in the spatial domain has an advantage because an unrestricted number of different spatial history samples can be obtained and joined into a test signal of any length without repetition in the data. Thus, a realistic variability of test conditions is provided throughout simulation that is lacking in the cycle replication of the same course profile record.

The Wave Number Spectrum

The most common approach to processing time history data



Aerial view of the Munson test area at Aberdeen Test Center and a HMMWV being evaluated on a hilly cross country course.

is to transform the signal to the frequency domain using the direct Fourier transform (normally in the form of FFT). That is how a PSD function describing distribution of the signal energy along the frequency axis is obtained. The same process can be established³ for the spatial data (like those shown in Figures 1, 3, 5 and 7) where the equal distance measurement intervals are equivalent to equal time increment intervals. The resultant spectrum introduced for spatial history data is called a Wave Number Spectrum (WNS) and examples are presented in Figures 2a, 4a, 6a and 8a.

The horizontal axis of WNS plots is the wave number and is equivalent to frequency in the time domain PSD. For the ATC terrain profile measurements made at intervals of $\Delta x = 0.25$ ft, the wave number has units of cycles per foot (or 1/ft). The course roughness (i.e., the displacement measured by the profilometer) is expressed in inches. Thus, the variance of the terrain profile signal (i.e., the area under the WNS curve) has units of in.^2 . Likewise, the area under the PSD curve of an acceleration signal has units of $(\text{m/s}^2)^2$.

If the area under the WNS curve is in in.^2 and the horizontal axis has units of 1/ft then the vertical axis of the wave number spectrum will be in $\text{in.}^2/(\text{1/ft})$, i.e., displacement squared divided by the analysis bandwidth (cycles per foot). A wave

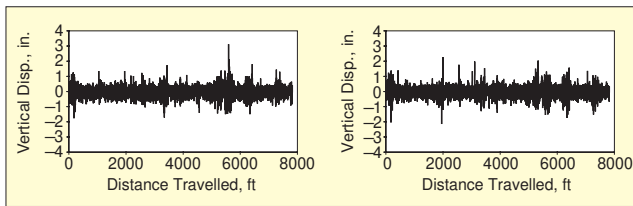


Figure 1. Terrain profile spatial histories measured on Course A (left and right tracks).

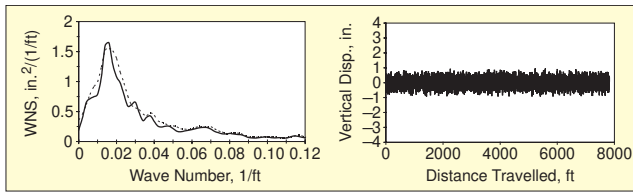


Figure 2. Results of the Fourier transform simulation for Course A. Left – WNS of real terrain profile (solid curve) and WNS of synthetic terrain signal (dotted curve). Right – spatial history of synthetic terrain signal generated from WNS.

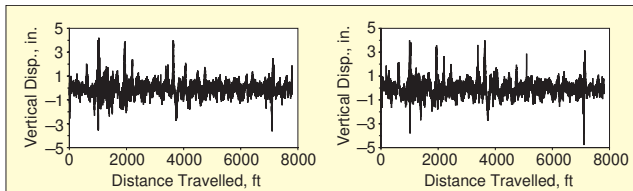


Figure 3. Terrain profile spatial histories measured on Course B (left and right tracks).

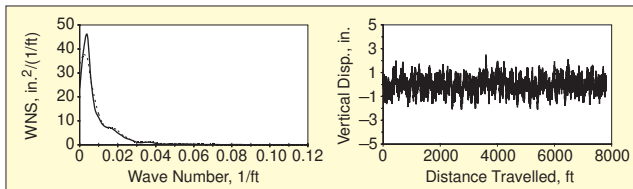


Figure 4. Results of the Fourier transform simulation for Course B. Left – WNS of real terrain profile (solid curve) and WNS of synthetic terrain signal (dotted curve). Right – spatial history of synthetic terrain signal generated from WNS.

number spectrum obtained for a given course profile can be converted into a displacement PSD at the tire/road interface for a particular vehicle speed and, then, to an acceleration PSD at the tire/road interface.³ Hence, different speeds produce different frequency domain spectra from the same wave number spectrum. The resultant spectrum is a “point follower” representation of the tire/road interface and does not include tire or vehicle dynamics.

Simulating Terrain Profiles by Fourier Transform

Four ATC test courses have been analyzed and are referred to below as Courses A, B, C and D. The spatial histories of the left and right tracks for each of the courses are presented in Figures 1, 3, 5 and 7. The corresponding left and right track profiles look similar and their WNSs appear to be close to each other. The solid line on Figures 2a, 4a, 6a and 8a depicts the WNS of the left track for each of the courses.

The WNS spectra obtained were subjected to an inverse Fourier transform procedure and synthetic spatial histories were

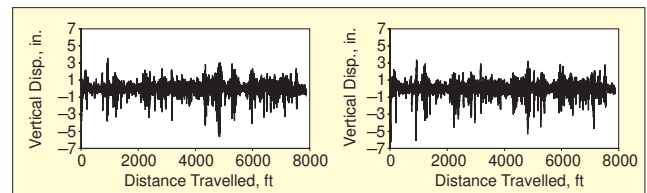


Figure 5. Terrain profile spatial histories measured on Course C (left and right tracks).

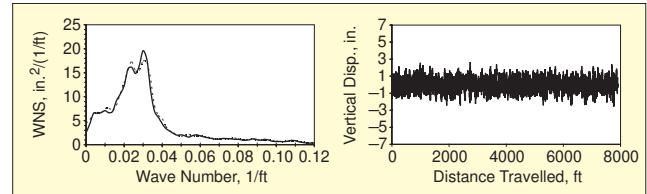


Figure 6. Results of the Fourier transform simulation for Course C. Left – WNS of real terrain profile (solid curve) and WNS of synthetic terrain signal (dotted curve). Right – spatial history of synthetic terrain signal generated from WNS.

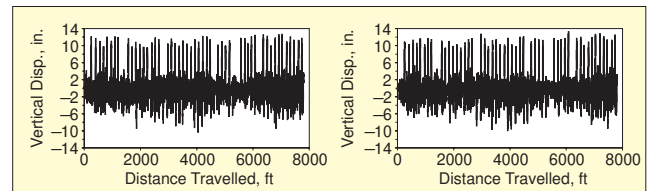


Figure 7. Terrain profile spatial histories measured on Course D (left and right tracks).

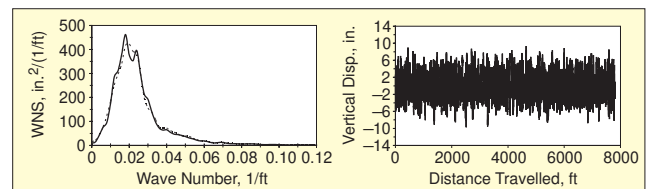


Figure 8. Results of the Fourier transform simulation for Course D. Left – WNS of real terrain profile (solid curve) and WNS of synthetic terrain signal (dotted curve). Right – spatial history of synthetic terrain signal generated from WNS.

calculated. The latter are shown in Figures 2b, 4b, 6b and 8b, and appear to differ dramatically from the initial course profile records depicted in Figures 1, 3, 5 and 7. It is obvious that the synthetic spatial histories generated have lost their severity compared to the real terrain data. Table 1 contains values of the highest positive/negative peaks in the course terrain profiles and the synthetic spatial histories for all four courses. It can be seen from the ratios between the corresponding highest peaks that the simulation by common direct/inverse Fourier transform in the spatial domain provides several times less severe roughness than that of the real terrain. Similar or higher differences will remain in corresponding velocity and acceleration records at the tire/road interface.

The objective of this article is to study and improve the above unsatisfactory comparison. First, the closeness in terms of the WNS was re-examined as the synthetic spatial histories generated were subjected to direct Fourier transformation to convert them back to the wave number domain. The resulting WNSs of the synthetic signals, shown by dotted lines in Figures 2a,

Table 1. Comparison of highest positive/negative peaks in the course profiles and the Fourier-simulated synthetic spatial histories.

		Course A		Course B		Course C		Course D	
		Left Track	Right Track	Left Track	Right Track	Left Track	Right Track	Left Track	Right Track
Highest Positive Peak	Terrain Profile	3.1 in.	2.3 in.	4.2 in.	4.0 in.	3.9 in.	4.3 in.	13.4 in.	12.6 in.
	Fourier Simulation	0.9 in.	0.9 in.	2.4 in.	2.4 in.	2.6 in.	2.8 in.	9.2 in.	9.2 in.
	Ratio	3.4	2.6	1.75	1.67	1.5	1.53	1.46	1.37
Highest Negative Peak	Terrain Profile	-1.8 in.	-2.1 in.	-3.6 in.	-4.7 in.	-5.6 in.	-6.3 in.	-10.1 in.	-10.3 in.
	Fourier Simulation	-0.9 in.	-0.9 in.	-2.1 in.	-2.1 in.	-2.5 in.	-2.7 in.	-9.6 in.	-9.6 in.
	Ratio	2.1	2.3	1.7	2.24	2.24	2.33	1.05	1.07

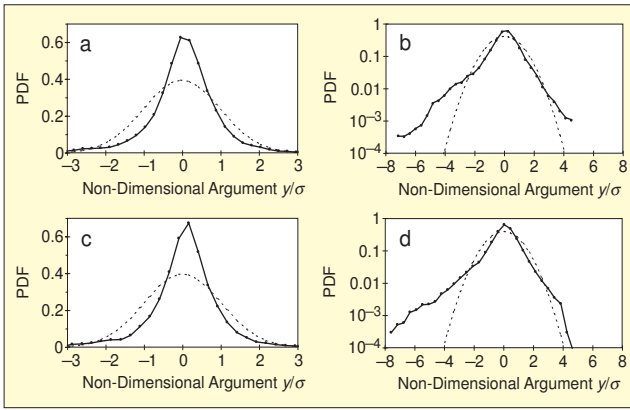


Figure 9. Experimental PDF of terrain profile for Course C (solid line) and Gaussian model (dotted line). a – central section for the left track ($\lambda = -1.0, \gamma = 8.0$), b – tails for the left track, c – central section for the right track ($\lambda = -1.3, \gamma = 9.7$), d – tails for the right track.

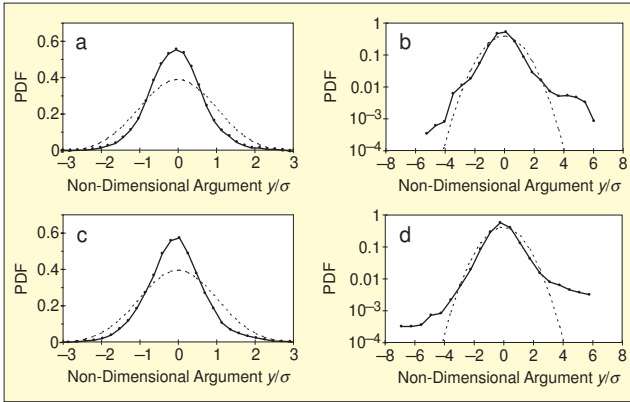


Figure 10. Experimental PDF of terrain profile for Course B (solid line) and Gaussian model (dotted line). a – central section for the left track ($\lambda = 1.0, \gamma = 9.0$), b – tails for the left track, c – central section for the right track ($\lambda = 1.0, \gamma = 9.8$), d – tails for the right track.

4a, 6a and 8a, are sufficiently close to the initial WNSs of the experimental road data. Hence, the above difference in peak behavior is not attributed to the WNS approach. Other characteristics of random processes should be implemented in addition to WNS to describe the difference between the experimental and synthetic spatial histories.

Probability Density Function Analysis

It is known from the time data analysis that the PSD is a sufficient description of stationary random signals only if the process under consideration is Gaussian. If it is not, then the Probability Density Function (PDF) must be computed and its deviations from the Gaussian model

$$P_G(u) = \frac{1}{\sigma\sqrt{2\pi}} \exp\left[-\frac{(u-m)^2}{2\sigma^2}\right] \quad (1)$$

must be studied. The principal characters describing non-Gaussian PDF features are skewness and kurtosis

$$\lambda = \frac{M_3}{(M_2)^{3/2}} = \frac{M_3}{\sigma^3}, \quad \gamma = \frac{M_4}{(M_2)^2} = \frac{M_4}{\sigma^4} \quad (2)$$

governed by central moments $M_k = \int_{-\infty}^{\infty} (u-m)^k P(u) du$ of the probability density function $P(u)$.

The Gaussian distribution (Eq. 1) is specified by two parameters: mean value m and variance σ^2 , where the latter coincides with the second moment M_2 . However, there is no variability in PDF moments higher than the second. The skewness and kurtosis related to the third and fourth moments are constants ($\lambda = 0, \gamma = 3$) for the Gaussian PDF. Hence, any other λ and γ values obtained would be an indication of Gaussian model failure, i.e., a suggestion about limitations on the use of the Fou-

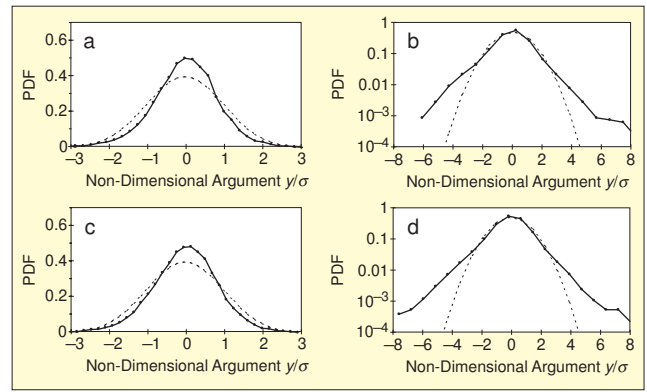


Figure 11. Experimental PDF of terrain profile for Course A (solid line) and Gaussian model (dotted line). a – central section for the left track ($\lambda = -0.2, \gamma = 7.0$), b – tails for the left track, c – central section for the right track, ($\lambda = -0.2, \gamma = 6.2$), d – tails for the right track.

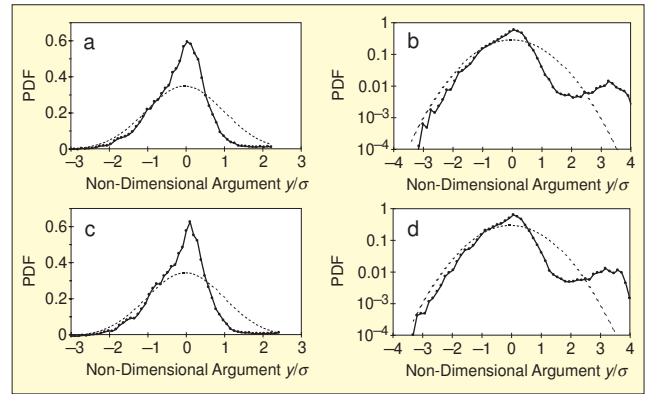


Figure 12. Experimental PDF of terrain profile for Course D (solid line) and Gaussian model (dotted line). a – central section for the left track ($\lambda = 1.2, \gamma = 6.2$), b – tails for the left track, c – central section for the right track ($\lambda = 1.2, \gamma = 6.2$), d – tails for the right track.

rier transform approach. Such a situation has been discussed for time data records (acceleration), mainly for kurtosis deviations from the Gaussian model^{4,5} and also for skewness deviations.^{6,7} Both these types of non-Gaussian deviations have been observed in various vehicles.

An increase in the kurtosis of vehicle vibration data indicates the occurrence of unusually high peaks in the data set. The Gaussian model covers peaks up to some four or five root-mean-square (RMS) values. However, peaks higher than that have been found to be typical in vibration records measured in trucks, military trailers^{4,8} and automobiles.⁵ It is clear that an excessive peak in vibration is a consequence of some extreme irregularity at some point of the road or terrain.

Obviously, when peaks become radically different than those expected for the averaged RMS level, the course severity increases. This is commonly described by the crest factor

$$c = \frac{\max}{\sigma} \quad (3)$$

that is a ratio between the magnitude of the largest peak and the RMS value σ . However, the kurtosis is affected by all excessive peaks, not just the largest, as is the crest factor (Eq. 3). Therefore, the kurtosis value is a more robust characteristic than the crest factor.

When working with kurtosis, special attention must be devoted to elimination of so-called ‘wild’ points. This is a typical problem when the data set becomes contaminated with one or more erroneously outlying points induced by the data acquisition system. It was reported⁴ that the presence of wild points changes the kurtosis to values comparable with those inherent of real field data. Since the kurtosis value is used as a description of vibration severity related to non-Gaussian peaks in the time history, it is necessary to distinguish a real kurtosis increase from that caused by erroneous wild points

and to correct them by data editing before subsequent analysis of non-Gaussian behavior.

Rougher road conditions and greater than expected number of excessive peaks mean that the probability of a certain peak occurrence (i.e., PDF) increases compared to the probability of the same peak in a Gaussian process. Following the aforementioned results for vibration data, it is also desirable to quantify this effect in terrain profile data to numerically define limitations on the use of the wave number spectrum.

As the above relates to high peaks, the PDF increase takes place at the tails of the probability distribution. Thus, careful investigation of the PDF tail behavior becomes essential. The higher the peak, the less frequently it occurs. Hence, longer data records are necessary to have a representative statistical sample and to calculate the experimental PDF tails properly. Whether the distribution tails are non-Gaussian cannot be visually determined on PDF graphs with regular linear scales. To analyze this effect, one needs to present the PDF on a logarithmic scale (see Figures 9-12), which magnifies differences of theoretical and experimental probabilities for high amplitude values. Note that the left and right tails will be different if the PDF is asymmetric.

PDFs of the Course Terrain Data

The course data analysis algorithm concentrated on determination of the instantaneous-value PDFs (or as they are sometimes called “amplitude PDFs”) and calculation of skewness and kurtosis values (Eq. 2). The moment characteristics were found by time averaging

$$M_k^y = \frac{1}{n} \sum_{i=1}^n [y(i\Delta x) - m]^k, \quad m = \frac{1}{n} \sum_{i=1}^n y(i\Delta x) \quad (4)$$

as for an ergodic random process. The number of points in the course profile spatial records $y(x)$ was 30,000-40,000.

Since the step character of a histogram (a PDF estimation from data) makes comparison with the Gaussian curve difficult, the experimental PDFs are plotted in the form of a curve connecting vertices of the histogram bins (Figures 9-12 and 14). The PDFs are often presented in non-dimensional form, where the horizontal axis represents a ratio between instantaneous values and the RMS value. Such a presentation is used in this section (Figures 9-12) to simplify comparison with the Gaussian model.

As the importance of PDF tail behavior for the course profiles has been outlined in the previous section, each PDF is shown in two graphs. One of them depicts the PDF central section on the regular linear scale for the vertical axis, and the other shows the distribution tails on a logarithmic scale (the horizontal axis of the PDF arguments is always linear).

All spatial histories of the course profiles presented in Figures 1, 3, 5 and 7 have been subjected to the PDF and skewness/kurtosis analysis. The experimental PDFs computed (solid lines in Figures 9-12) were compared with the Gaussian distribution (Eq. 1) shown by the dotted line. The skewness λ and kurtosis γ values obtained are given in the captions. It appears that terrains of the four test courses under consideration are non-Gaussian random processes. This is evident from the PDF graphs and from the skewness and kurtosis values which were far from Gaussian ($\lambda = 0$, $\gamma = 3$). As could be expected, the degree and nature of non-Gaussian behavior is always similar for left and right tracks of the same course.

Course C has negative skewness of $\lambda = -1.15$, which is an evidence of very strong non-Gaussianity, and is much larger than typical skewness values for acceleration data. The left PDF tail, up to -8σ values, is much longer than the right tail, which does not exceed 5σ (see Figures 9b and 9d). This is the reason for the large skewness value as there is no sign of asymmetry in the central section of the PDF shown in Figures 9a and 9c. Physically, the above means that trenches on the surface of this course are sharper than bumps. The aforementioned -8σ and 5σ tail lengths refer to crest factor values which, in the case of asymmetrically distributed data, should be treated separately

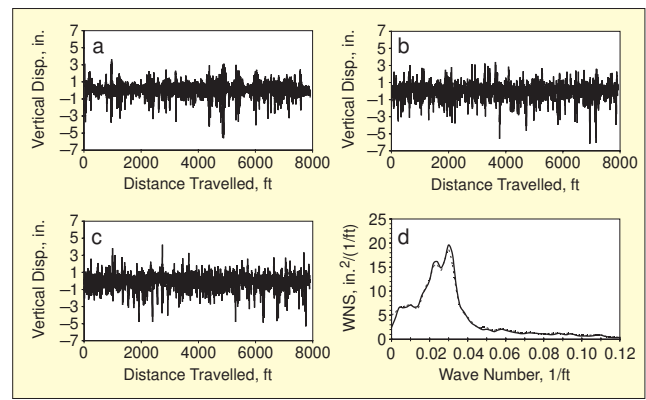


Figure 13. Comparison of terrain profile from Course C and simulated non-Gaussian terrain signals. a – spatial history measured on the test course, b – spatial history #1 by non-Gaussian simulation, c – spatial history #2 by non-Gaussian simulation, d – WNS of real terrain profile (solid curve) and WNS of simulated terrain signal (dotted curve).

for positive and negative peaks, i.e. $c_+ = 5$ and $c_- = 8$.

For Course B, the situation is the opposite; skewness is also large, about $\lambda = 1.0$, but positive. The central PDF section is almost symmetrical as for Course C. However, the PDF limits of Course B in Figures 10b and 10d are about the same at the left and at the right (approximately 6σ), contrary to what was the case for Course C. The difference for the PDF tails of Course B is not their length, but their height. The PDF values at the right tail (i.e., probability of bump occurrence) are 10 times larger on average (see Figures 10b and 10d) than at the left tail (i.e., probability of trench occurrence). The above means that for this course the bumps and trenches are of similar sharpness, but the bumps are encountered more frequently than the trenches.

Course A does not have a notable skewness ($\lambda = -0.2$) but it is also non-Gaussian as is reflected in the kurtosis of $\gamma = 6.6$ (on average). This value is smaller than those for Courses B and C ($\gamma = 8.8$ and $\gamma = 9.4$, respectively) but it is still significantly larger than the Gaussian value of $\gamma = 3.0$. The PDF tails (see Figures 11b and 11d) are both extended to 8σ , i.e., crest factor is $c_+ \approx c_- = 8$, compared to $c = 3.5-4.0$ for the Gaussian data of a similar record length.

The PDF of Course D is qualitatively different from all others as it is bimodal. The second additional PDF peak occurs for positive arguments in the region of $3.0-3.5\sigma$ (see Figures 12b and 12d). This is caused by frequent bumps on the road which are approximately of the same height and clearly visible in the graphs of the terrain profile (Figure 7). These peaks in the spatial histories are not erroneous outliers as each of the bumps consists of several data points – not a single point as a typical outlier would. Obviously, the additional PDF increase on just one of two sides of the main PDF peak introduces essential skewness, that is $\lambda = 1.2$ for this course. There are no long tails (see Figures 12b and 12d) and all data are located within an interval of $[-4\sigma, +4\sigma]$ corresponding to the Gaussian crest factor. Nevertheless, the kurtosis value is non-Gaussian ($\gamma = 6.2$ on average). This increase of kurtosis is because of the contribution of higher probability of those amplitude terrain values that are at the additional PDF peak.

Non-Gaussian Simulation of the Test Course Terrain

Results of the PDF analysis presented in the above section clarify non-Gaussian behavior of the course terrain data and allow an approach to the problem of simulation for experimen-

Table 2. PDF characteristics and crest factors for the measured Course C profile and synthetic spatial histories generated.

Characteristic	Skewness	Kurtosis	Crest factor	
			Positive	Negative
Course C Profile (Left Track)	-1.0	8.0	4.7	-7.3
Non-Gaussian Simulation	-1.1	8.05	4.5	-8.2
Fourier Simulation	-0.07	2.9	3.15	-3.5

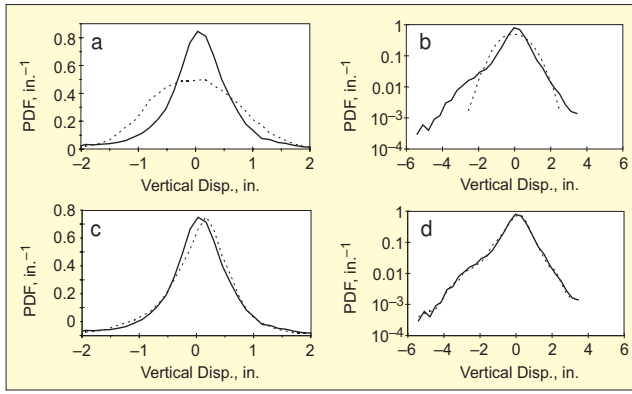


Figure 14. PDF of terrain profile on Course C (solid line) and PDFs of simulated terrain signals (dotted). a – Fourier simulation (central PDF section), b – Fourier simulation (PDF tails), c – non-Gaussian simulation (central PDF section), d – non-Gaussian simulation (PDF tails).

tal testing or numerical modeling. A number of non-Gaussian simulation methods have been developed^{5,6,9,10} for electro-dynamic shaker testing, i.e., for digital generation of non-Gaussian time histories. All these methods can be applied in the spatial domain by using the WNS instead of the PSD.

Most of the previous work is based on nonlinear transformation of a Gaussian random process with the given PSD, and that will be implemented first for the terrain data. The objective is to achieve the prescribed values of skewness λ and kurtosis γ simultaneously with the given WNS. To operate with non-Gaussian moment characteristics like λ and γ , the Hermite polynomial model of a nonlinear transform function suggested by Winterstein¹¹

$$\frac{y-m}{\sigma} = \tilde{y} = F(z) = h[z + a(z^2 - 1) + b(z^3 - 3z)] \quad (5)$$

is particularly useful.

In Eq. 5, an argument z of the nonlinear transformation function $F(z)$ is supposed to be some Gaussian random process $z(x)$ with unit variance. This process $z(x)$ is transformed by function $F(z)$ into the simulated non-Gaussian spatial history of the course terrain $y(x)$ considered in Eq. 4. The intermediate variable is a result of standardization and centralizing of the spatial history $y(x)$ with respect to its mean m and RMS σ values. Coefficients a and b can be chosen such that the non-Gaussian random process $y(x)$ obtained has the specified skewness λ^* and kurtosis γ^* values. Analytical relations between a , b and λ^* , γ^* were given in¹¹

$$a = \frac{\lambda^*}{4 + 2\sqrt{1 + 1.5(\gamma^* - 3)}}, \quad b = \frac{\sqrt{1 + 1.5(\gamma^* - 3)} - 1}{18} \quad (6)$$

and the scaling factor h has been also found

$$h = \frac{1}{\sqrt{1 + 2a^2 + 6b^2}} \quad (7)$$

from the condition that the standardized intermediate non-Gaussian random process must have unit variance.¹¹

The above nonlinear transformation procedure has been implemented to numerically simulate test Course C, whose spatial history is shown in Figure 5 at the left and whose PDF is presented in Figures 9a and 9b. For the Course C left track with skewness $\lambda^* = -1.0$ and kurtosis $\gamma^* = 8.0$, Eqs. 6 and 7 give following values of the coefficients for the nonlinear transform (Eq. 5)

$$a = -0.102, \quad b = -0.106, \quad h = 0.959 \quad (8)$$

To serve as an input for the Hermite polynomial transformation, the Gaussian random process $z(x)$ can be naturally taken from spatial histories generated by the regular inverse Fourier transform for the given WNS of the test course under consideration. One such spatial history is shown in Fig 6b with its WNS close to the WNS of the measured terrain profile (see

Figure 6a). After this Gaussian synthetic spatial history was subjected to the nonlinear transform (Eq. 5) with coefficients (Eq. 8), the non-Gaussian spatial history obtained (Figure 13b) appears to be similar to the measured data (Figure 13a), which was not the case with the common Fourier simulation (see Figures 5 and 6b).

To compare Gaussian and non-Gaussian simulation in terms of PDF, the latter has been calculated for the Fourier-generated (Figure 6b) and Hermite-polynomial-generated (Figure 13b) spatial histories. The result is shown in Figure 14 with the horizontal axis representing real surface roughness in inches (no standardization to the non-dimensional argument y/σ). Both for the central PDF section (Figures 14a and 14c) and the tails (Figures 14b and 14d), the non-Gaussian approach improves simulation dramatically and allows a precise fit of the experimental PDF, which was impossible with the regular Fourier simulation. For example, at the left tail for probabilities of 0.0006 in.⁻¹, the non-Gaussian method matches the value of 5 in. observed for the given PDF of the measured data (left edge of solid and dotted curves in Figure 14d), whereas the Fourier simulation provides the smaller value of less than 3 in. (see dotted curve in Figure 14b).

The difference between the precision of Gaussian and non-Gaussian approaches is also essential in the results presented in Table 2 where the skewness, kurtosis and crest factor characteristics of simulation data are compared with those of the prescribed terrain profile. As discussed in the PDF Analysis section, the skewness and kurtosis values of the Gaussian Fourier-generated data are close to $\lambda = 0$ and $\gamma = 3$ (see last row in Table 2), whereas the skewness and kurtosis of the measured terrain profile are very much different. They, however, have been achieved by the non-Gaussian simulation (see the second row in Table 2). The outcome of the non-Gaussian approach in terms of crest factor results is given in the last two columns of Table 2. The positive c_+ and negative c_- crest factor values are distinct in non-Gaussian data exactly like in the real terrain profile. For the Fourier-generated data, the positive and negative crest factors were about the same and much less than in the real data (see Table 2).

In the above context, the crucial point is that the synthetic non-Gaussian spatial history generated is not unique as another one can be obtained from the next Fourier-generated spatial history sample taken as an input for the nonlinear transformation (Eq. 5). It was mentioned in the introduction that an important advantage of the Fourier simulation is that a test signal of any length can be generated without repetitions in the data (such repetitions are inevitable if the measured spatial history is simply cycled during the test). Now the same realistic variability of test conditions can be achieved with more precise non-Gaussian simulation. This can be carried out as follows.

An unrestricted number of different Gaussian spatial history samples, all with the same WNS, are available as a result of Fourier simulation. Each of these Gaussian spatial histories is then subjected to the nonlinear transform (Eq. 5), producing its specific non-Gaussian output with all characteristics (not only WNS) close to those of the terrain data prescribed. Hence any necessary number of different non-Gaussian spatial history samples can be obtained. Two of them are shown in Figures 13b and 13c, both similar to the prescribed terrain data in Figure 13a, but different from each other. The same will be the case for other non-Gaussian samples.

It should be mentioned that a nonlinear transform of a random process, like that given by Eq. 5, not only changes the PDF (that was our objective) but also affects the frequency spectrum, or WNS in the spatial case (an undesired effect). As a result, the precision of WNS modelling after non-Gaussian simulation may worsen compared to that of Fourier simulation. However, for the Course C terrain under consideration, WNS of the non-Gaussian simulation data shown by the dotted curve in Figure 13d appeared to be as close to the WNS of the measured terrain as the WNS of Fourier-generated data were in Figure 6a.

If it were not the case, an iteration procedure of input spectrum correction could be implemented.^{5,10}

References

1. Haug, E. J., Negrut, D., Serban, R., Solis, D., "Numerical Methods for High-Speed Vehicle Dynamic Simulation," *Mechanics of Structures and Machines*, Vol. 27 (4), 1999, pp 507-533.
2. De Cuyper, J. and Coppens, D., "Service Load Simulation on Multi-Axis Test Rigs," *Sound and Vibration*, October 1999, pp 30-35
3. Connon, W. H., "Determining Vehicle Sensivity to Changes in Test Course Roughness," *Proceedings of the 46th IEST Annual Technical Meeting*, Providence, RI, 2000, pp 204-216.
4. Connon, W. H., "Comments on Kurtosis of Military Vehicle Vibration Data," *Journal of the Institute of Environmental Sciences*, No. 6, September/October, 1991, pp 38-41.
5. Steinwolf, A., "Shaker Simulation of Random Vibrations with a High Kurtosis Value," *Journal of the Institute of Environmental Sciences*, No. 3, May/June, 1997, pp 33-43.
6. Steinwolf, A., "Bench Dynamic Test for Vehicle Random Vibrations with Asymmetrical Probability Distribution," *Proceedings of the 26th Int. Symposium on Automotive Technology and Automation (Dedicated Conference on Mechatronics)*, Aachen, 1993, pp 711-718.
7. Steinwolf, A. and Ibrahim, R. A., "Analysis and Simulation of Asymmetric Probability Distributions During Fundamental and Environmental Random Vibration Tests," *Proceedings of the 43rd IEST Annual Technical Meeting*, Los Angeles, 1997, pp 48-55.
8. Charles, D., "Derivation of Environment Descriptions and Test Severities from Measured Road Transportation Data," *Environmental Engineering*, December, 1992, pp 30-32; March, 1993, pp 25-26.
9. Merritt, R. G., "A Stochastic Model for the Pulse Method – Part 2: Random Part," *Proceedings of the 43rd IEST Annual Technical Meeting*, Los Angeles, 1997, pp 121-129.
10. Smallwood, D. O., "Generation of Stationary Non-Gaussian Time Histories with a Specified Cross-Spectral Density," *Shock and Vibration*, Vol. 4, 1997, pp 361-377.
11. Winterstein, S. R., "Nonlinear Vibration Models for Extremes and Fatigue," *ASCE Journal of Engineering Mechanics*, Vol. 114, 1988, pp 1772-1790. 

The authors can be contacted at: a.steinwolf@auckland.ac.nz and william.connon@atc.army.mil.